Clays and Clay Minerals (2024), **72**, e26, 1–9
doi:10.1017/cmn.2024.15

Original Paper

Factors governing Fe^{2+}-catalyzed transformation of ferrihydrite associated with kaolinite under anoxic conditions

Cong Wu, Shuai Wang, Wenjuan Liao and Hao-Jie Cui
Yuelushan Laboratory, College of Resources, Hunan Agricultural University, Changsha 410128, China

Abstract

Fe^{2+}-catalyzed transformation of poorly crystalline ferrihydrite into highly crystalline forms is critical in the biogeochemical cycles of Fe, nutrients, and trace elements. The co-existence of ferrihydrite and kaolinite is widespread in soils of tropical and subtropical regions. In this investigation, three associations of ferrihydrite–kaolinite with ratios of 10, 30, and 50% (10% Fhy–Kln, 30% Fhy–Kln, and 50% Fhy–Kln) were examined to study the impact of the initial Fe^{2+} concentration and pH on Fe^{2+}-catalyzed transformation under anoxic conditions. The findings reveal that the ferrihydrite in the 10% Fhy–Kln associations has the smallest particle size and the largest number of surface hydroxyl groups. At 0.5 mM Fe^{2+} and pH 7.5, ferrihydrite underwent transformation into lepidocrocite, with the presence of kaolinite promoting the formation of goethite. Moreover, the presence of kaolinite influenced the morphology of the resulting transformation products. A decrease in pH hindered the transformation of ferrihydrite, while an increase in Fe^{2+} concentration resulted in the formation of magnetite. The impact of kaolinite in the association system on the transformations of ferrihydrite occurs primarily through alteration of the properties of ferrihydrite during its formation process.

Keywords: associations; Fe^{2+}-catalyzed transformation; ferrihydrite; kaolinite

(Received: 12 December 2023; revised: 11 March 2024; accepted: 12 April 2024)

Introduction

Ferrihydrite nanoparticles, which are Fe-(oxyhydr)oxides, are widely distributed in soils and sediments (Laurel et al., 2019; Iorio et al., 2022; Zhang et al., 2023a). Due to their small particle size, large specific surface area, and abundant surface sites, ferrihydrite is commonly considered an important contaminant and nutrient sink in soils and sediments (Wang et al., 2016; Huang et al., 2020; Mendez et al., 2020). Ferrihydrite nanoparticles are widely acknowledged to exhibit metastable characteristics due to their low crystallinity, and ferrihydrite transforms to crystalline Fe-(oxyhydr)oxides in the presence of aqueous Fe^{2+} under anoxic conditions. The Fe(II) adsorbed on the surface of ferrihydrite undergoes electron exchange with the structural Fe(III) of ferrihydrite, causing dissolution and subsequent precipitation of ferrihydrite, leading to its transformation into lepidocrocite and goethite. The transformation of ferrihydrite, catalyzed by the presence of Fe^{2+}, is subject to various factors, such as the concentration of Fe^{2+}, temperature, pH, and the presence of organic matter, within the reaction system (Hansel et al., 2005; Sheng et al., 2020; Yan et al., 2021; Liu et al., 2023). At high pH and high Fe^{2+} concentrations, ferrihydrite transforms into magnetite (Aeppli et al., 2019; Liu et al., 2023). Under conditions of weakly acidic pH and low Fe^{2+} concentration, ferrihydrite tends to transform into lepidocrocite and goethite (Hansel et al., 2005; Sheng et al., 2020). Elevated temperatures can induce ferrihydrite to transform into hematite (Yan et al., 2021), while the presence of chloride ions facilitates the transformation of ferrihydrite into lepidocrocite (Hansel et al., 2005). The co-existence of organic matter and arsenic impedes the transformation of ferrihydrite (Cai et al., 2020; Zhou et al., 2021). This transformation process significantly influences the speciation and bioavailability of heavy metal pollutants (Shi et al., 2021). As ferrihydrite transitions to crystalline iron forms, heavy metals such as cadmium, arsenic, or chromium, initially associated with ferrihydrite, are released from the solid to the liquid phase, enhancing their mobility (Hu et al., 2019; Zhao et al., 2022a; Zhao et al., 2022b). Concurrently, the formation of crystalline iron phases facilitates the immobilization of these heavy metals from the liquid phase into the crystalline structure, thereby mitigating their bioavailability (Zhao et al., 2022a; Zhao et al., 2022b).

Kaolinite, a prominent clay mineral, is found extensively in soils of tropical and subtropical regions (Ryan and Javier, 2013; Gilkes and Prakongkep, 2016). Under anoxic conditions, kaolinite can adsorb Fe^{2+} (Bhattacharyya and Sen, 2009) or be associated with Fe-(oxyhydr)oxides (Van et al., 2020) and consequently influence the reaction of the Fe^{2+}-catalyzed transformation of ferrihydrite (Meng et al., 2022). The study reveals that interactions between kaolinite and ferrihydrite, including electrostatic adsorption,

Corresponding author: Hao-Jie Cui; Email: hjcui@hunau.edu.cn
Cite this article: Wu C., Wang S., Liao W., & Cui H.-J. (2024). Factors governing Fe^{2+}-catalyzed transformation of ferrihydrite associated with kaolinite under anoxic conditions. *Clays and Clay Minerals* **72**, e26, 1–9. https://doi.org/10.1017/cmn.2024.15

hydrogen bonding, and chemical bonding, play a significant role (Yan et al., 2021; Han et al., 2024). The presence of kaolinite can inhibit the transformation of ferrihydrite into crystalline iron oxide during aerobic aging (Fan et al., 2023; Han et al., 2024) and also affects the aggregation and structural rearrangement of ferrihydrite during dehydroxylation on the surface of kaolinite (Zhang et al., 2023b; Han et al., 2024). Moreover, in the anoxic aging system of Fe^{2+}/Fe^{3+} and the presence of kaolinite, the formation of Fe^{2+}-accelerated catalytic Fe-(oxyhydr)oxides and kaolinite associations is hindered (Wei et al., 2011). With a pH range from 5 to 9, associations of goethite–kaolinite, hematite–kaolinite, and magnetite–kaolinite are formed. Additionally, with R (molar ratio of Fe^{2+}/Fe^{3+}) ranging from 0 to 0.5, the presence of crystalline Fe-(oxyhydr)oxides varies from non-existent to existent, and with an increase in the value of R, the occurrence of magnetite increases. The effect of co-existing minerals on the Fe^{2+}-catalyzed transformation of ferrihydrite under anoxic environments, especially in the presence of kaolinite, remains inadequately understood. The hypothesis stated that the relative proportion of kaolinite, the concentration of Fe^{2+}, and the pH level are crucial in determining the formation of specific Fe-(oxyhydr) oxides. Thus, the aim of this research was to examine the impact of kaolinite on the anoxic transformation of ferrihydrite into other Fe-(oxyhydr)oxides, to gain a better understanding of the role of kaolinite in the iron cycle.

In this investigation, three associations with varying proportions of kaolinite were prepared to study the recrystallization process of ferrihydrite under various Fe^{2+} concentrations and pH levels in anoxic conditions. Comparisons were drawn between the transformation processes in the kaolinite-associated system and the pure ferrihydrite system. The reaction characteristics and differences under various conditions were clarified.

Materials and methods

Preparation of kaolinite colloids

50 g of kaolinite was placed in a 2 L Pyrex beaker, then moistened with a small amount of deionized water, and reacted with 20 mL of 30% H_2O_2 at 40°C (heating in a water bath) to remove organic matter. No effervescence was observed after manual swirling, indicating that no H_2O_2 was present, and the sample was then washed five times with ethanol by centrifugation (10,000 rpm, 10 min, and 6050×g). The <2 μm particle-size fraction was then separated from the kaolinite by centrifuge washing (Day, 1965) at a speed of 10,000 rpm (10 min, 6050×g) and oven-dried at 40°C. The resulting powder was ground in an agate mortar, passed through a 0.15 mm sieve, and then stored in a desiccator for future use. All chemical reagent information is given in the Supplementary material (section 'Text S1').

Preparation of ferrihydrite–kaolinite associations

To prepare the associations, specific steps (Schwertmann and Cornell, 2008) were followed. Initially, precise quantities of $Fe(NO_3)_3{\cdot}9H_2O$ (0.8, 3.1, or 7.2 g) were weighed and dissolved in 150 mL of deionized water. Next, 1.8 g of kaolinite solid was weighed and subjected to sonication (200 W, 20 kHz) in 150 mL of deionized water for 30 min. The resulting kaolinite suspension was then added gradually to the iron nitrate solution under mechanical stirring. The pH of the mixture was adjusted to 7–8 using NaOH. Following this, the suspensions were centrifuged and washed several times with deionized water. The solids were subsequently freeze-dried, ground in an agate mortar, and sieved through a 0.15 mm sieve. These solids were stored in a desiccator for future use. The resulting associations were labelled as 10% Fhy–Kln, 30% Fhy–Kln, and 50% Fhy–Kln corresponding to the proportion of ferrihydrite in associations.

Sample analyses

10 mg of the associations were weighed precisely and placed in a 20 mL centrifuge tube, to which 10 mL of 6 M HCl was added to dissolve the solid. After a reaction time of 20 min, the suspension turned white, indicating the presence of residual kaolinite. Following the dissolution, the supernatant was separated through a centrifuge-filtration method, using a disposable 0.22 μm needle filter for the filtration process. Subsequently, the concentration of Fe was determined using the phenanthroline colorimetry method. The findings demonstrated that the proportions of ferrihydrite in the three different associations were 11.8, 30.5, and 49.8%, respectively, with the chemical formula of ferrihydrite being proposed as $Fe_5HO_8{\cdot}4H_2O$.

The minerals (to be used for determining the transformation rate of ferrihydrite) were extracted with 0.4 M HCl for a period of 6 h to assess the amount of ferrihydrite in the reaction process, and the total Fe content of the same minerals was extracted with 6 M HCl. The transformation percentage of ferrihydrite was further calculated as $Fhy\% = (1 - Fe_{0.4M\ HCl}/Fe_t)$ (Stookey, 1970; Zhao et al., 2022a).

Characterization

The mineralogical characteristics of the transformation products were analyzed using a Shimadzu-6100 X-ray diffractometer equipped with CoKα1 radiation (λ=0.1541 nm). The diffractometer settings included voltage of 40 kV, current of 30 mA, a scanning range 5–80°2θ, and a scanning speed of 8°2θ min^{-1}. The detailed procedure for preparing the powder X-ray diffraction samples is provided in the Supplementary material (section 'Text S2'). Fourier-transform infrared (FTIR) spectral data were obtained using a PerkinElmer Spectrum 65 FTIR spectrometer. For FTIR analysis, the specimens were dried and then compressed into tablets with KBr. Each FTIR spectrum was then obtained by accumulating 32 scans over a range from 4000 to 400 cm^{-1}, with a spectral resolution of 4 cm^{-1}. The morphologies of the synthesized products were observed using a ZEISS Sigma 300 field emission scanning electron microscope. Before examination, the specimens were fixed onto conducting tape and coated with a gold (Au) layer. The transformation products were further characterized by a FEI Tecnai F30 transmission electron microscope (TEM) operated at 200 kV, with samples deposited on a 300-mesh copper grid by dispersing ethanol. The adsorption characteristics of the associations were evaluated using the Brunauer–Emmett–Teller (BET) specific surface area test method, utilizing an automatic surface area and pore size distribution analyzer (BET SSA-4300). The samples were heated to 105°C for 6 h under a pressure of <1000 Pa. The pore structure was assessed at a low temperature of liquid nitrogen (77 K). Acid–base titration data were acquired using an electrochemical titration apparatus (Titrando-907, Metrohm, Switzerland), measuring the amount of acid consumed to determine sample properties at a background ionic strength of 0.1 M potassium chloride, with pH values ranging from 11 to 3.

https://doi.org/10.1017/cmn.2024.15 Published online by Cambridge University Press

Fe^{2+}-catalyzed transformation experiments

$FeCl_2$, sourced from Aldrich, was utilized to prepare a Fe^{2+} solution within a glovebox provided by Mikrouna Co., Ltd., China. The glovebox was filled with N_2 (99.999%) to ensure an oxygen concentration of <0.01 ppm. The preparation of deoxygenated water involved bubbling ultra-pure N_2 through deionized water in a 1 L reagent bottle for 2 h at room temperature, after which the bottle was sealed and placed inside the glovebox. The bottle was then left uncovered overnight in the anoxic glovebox to eliminate any remaining dissolved O_2. Experiments were conducted in a 20 mL glass bottle, which was sealed with a rubber stopper. The addition of experimental solid samples, buffer salts, and Fe^{2+} took place inside the glovebox to maintain an anoxic environment in the reaction bottle. After incorporating all reaction solutions into the glass bottle and sealing it with a rubber stopper, the bottle was transferred from the glovebox to a shaker for the reaction. A blank reaction system, containing Fe^{2+} and buffer salts, was used to ensure that the glass bottle remained free of O_2 throughout the reaction, thereby confirming the maintenance of an anoxic environment. The constant concentration of Fe^{2+} in the blank system, indicative of no Fe^{2+} oxidation, further confirmed the absence of O_2 during the reaction process.

The ferrihydrite concentration in the reaction system was controlled to 0.5 g L^{-1}, and three replicates were established for each reaction. After setting the reaction time (4, 12, 24, and 96 h), the samples were transferred to a glovebox to separate the solid and liquid phases. Subsequently, the solid samples were prepared for X-ray diffraction (XRD) and ferrihydrite transformation analysis. After 10 mL of filtrate was acidified with 50 μL of 3.6 M H_2SO_4 (to prevent the oxidation of Fe^{2+} in the subsequent aerobic environment), the filtrate was removed from the glovebox. The concentration of Fe^{2+} was then determined via the phenanthroline colorimetry method. The results revealed that after the acidified filtrate was taken out of the glovebox, the concentration did not change, indicating that the aerobic environment outside the glovebox did not affect the determination of the acidified filtrate.

The effect of various associated proportions of Fhy–Kln was investigated as follows: the initial concentration of Fe^{2+} was 0.5 mM, and the reaction pH was controlled at 7.5 with 25 mM 4-(2-hydroxyethyl)-1-piperazine-ethanesulfonic acid (HEPES). For the Fe^{2+} concentrations experiments, the pH of the reaction was maintained at 7.5, and 25 mM HEPES buffer was used while the initial Fe^{2+} concentrations were varied to 0.5, 1, or 2 mM. For the reaction pH experiments, the initial concentration of Fe^{2+} was 0.5 mM, and the initial pH was set as 5.5, 6.5, or 7.5. The initial pH was controlled with 25 mM 2-(N-morpholino) ethanesulfonic acid (MES), 1,4-piperazinediethanesulfonic acid (PIPES), or HEPES, respectively.

Results and Discussion

Characterization of the prepared associations

X-ray diffraction and scanning electron microscopy analysis

The XRD patterns of the synthesized Fhy–Kln associations (Fig. 1) revealed that their diffraction peaks closely resembled those of kaolinite, with no new diffraction peaks observed. This suggests that the association with ferrihydrite marginally affects kaolinite's crystalline structure. The XRD standard patterns of lepidocrocite, goethite, magnetite, and kaolinite are shown in Fig. S1 in the Supplementary material. However, as the ferrihydrite content increased from 10 to 50%, the intensity of kaolinite's diffraction

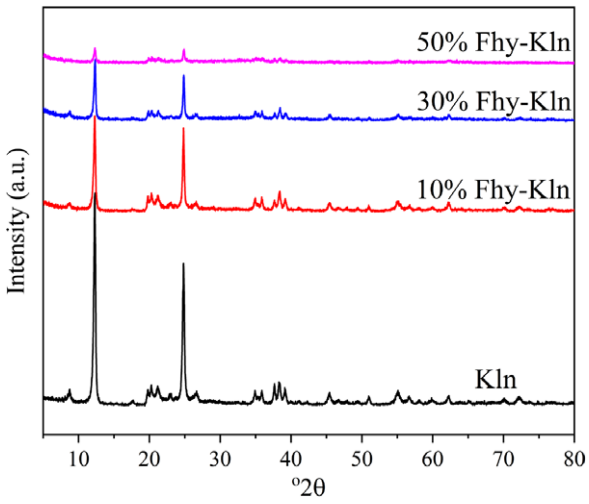

Figure 1. XRD patterns of kaolinite (Kln) and Fhy–Kln associations.

peaks within the associations diminished gradually, indicating the formation of amorphous ferrihydrite on the surface of kaolinite (Sun et al., 2022). Scanning electron microscopy (SEM) analysis was conducted to explore the association between ferrihydrite and kaolinite further, especially in terms of surface morphology changes. Compared with the smooth surface of pure kaolinite (Fig. S2a in the Supplementary material), the surfaces of kaolinites within the associations appeared rougher, with visible small ferrihydrite aggregates (Fig. S2b–d in the Supplementary material). The quantity of the iron oxide aggregates increased with the proportion of ferrihydrite in the associations, with some ferrihydrite aggregates existing independently.

BET analysis

BET analysis provided insights into the nitrogen isothermal adsorption and desorption behaviors of ferrihydrite and kaolinite (see Fig. S3a in the Supplementary material), revealing significantly higher nitrogen adsorption for ferrihydrite, which indicates a greater adsorption capacity compared with kaolinite (Kuila and Prasad, 2013; Thommes et al., 2015). The poresize distribution curve showed that both minerals contained primarily micropores of < 2 nm (see Fig. S3b in the Supplementary material), with ferrihydrite exhibiting a smaller average pore size than kaolinite. In Fhy–Kln associations (Fig. 2a; see also Fig. S3b in the Supplementary material), an increase in ferrihydrite content led to a gradual increase in nitrogen adsorption capacity and a significant increase in micropores, suggesting ferrihydrite's dominant role in adsorption without altering the poresize distribution. The specific surface areas of each sample (see Table S1 in the Supplementary material) revealed that the specific surface area of ferrihydrite far exceeds that of kaolinite, consistent with previous experimental findings (Gu et al., 2022; Zeng et al., 2023). Similarly, the specific surface area increases with increase in ferrihydrite in the associations. Furthermore, the specific surface area of the associations exceeded the value calculated from the sum of the proportional products of ferrihydrite and kaolinite (see Table S1 in the Supplementary material), results noted in a previous study also (Wei and Yang, 2010). As the pH value increased during the formation of associations, kaolinite not only bonded with ferrihydrite but also facilitated the dispersion of Fe in the solution, leading to the formation of ferrihydrite on the surface of kaolinite rather than its accumulation on existing ferrihydrite

https://doi.org/10.1017/cmn.2024.15 Published online by Cambridge University Press

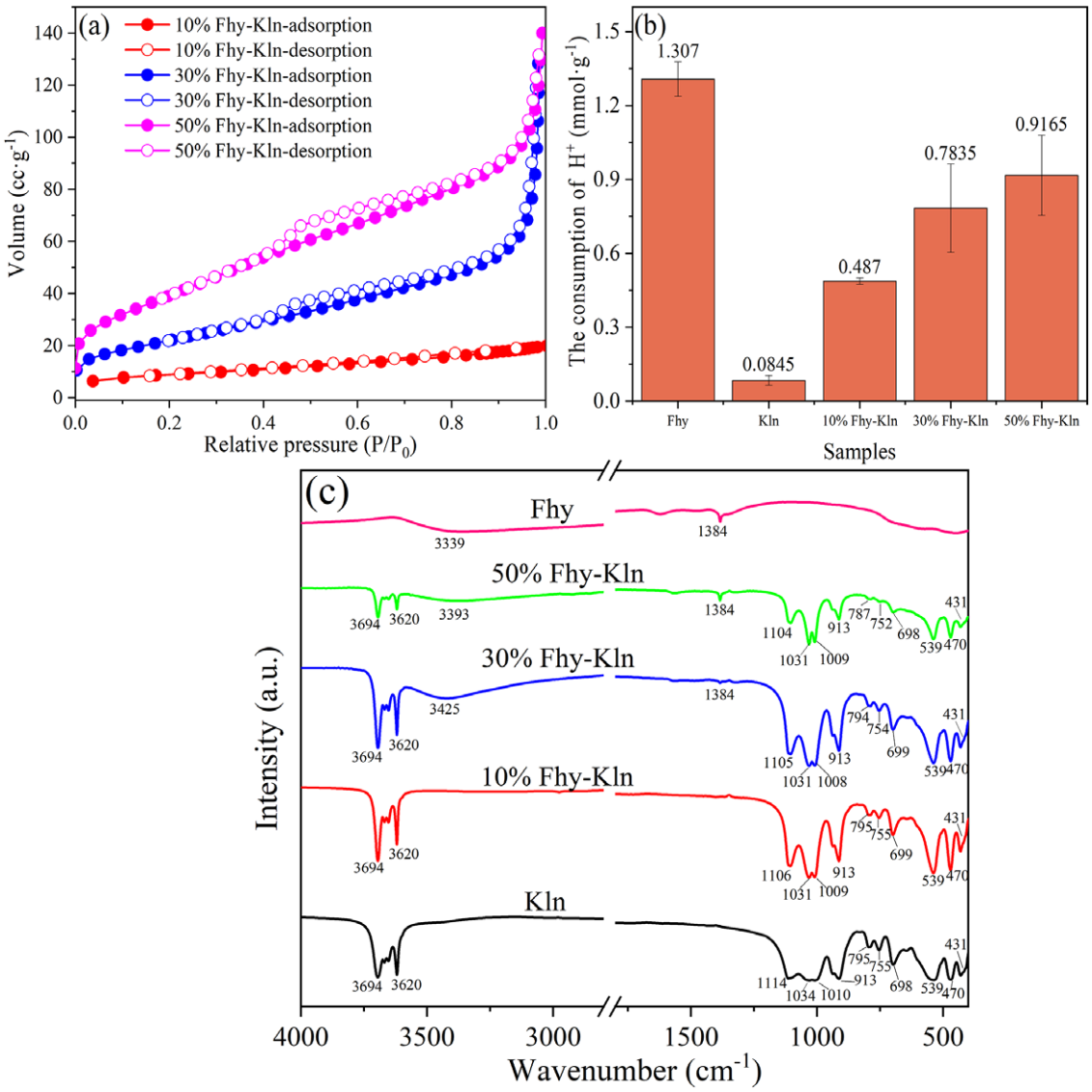

Figure 2. (a) Adsorption–desorption isotherms of Fhy–Kln associations; (b) H^+ consumption from pH 11 to pH 3 and (c) FTIR spectra of ferrihydrite (Fhy), kaolinite (Kln), and Fhy–Kln associations.

particles. This process resulted in the formation of smaller ferrihydrite particles at this stage.

Acid–base titration

The acid consumption (Fig. 2b) for each mineral was measured from pH 11 to pH 3, maintaining an ionic strength of 0.1 M. The consumption of acid correlates directly with the quantity of hydroxyl groups present on the surface of the mineral (Eren and Afsin, 2008; Gu and Evans, 2008). The comparison of acid consumption between minerals revealed that pure ferrihydrite consumes 15.5 times more acid than pure kaolinite, indicating that ferrihydrite possesses a significantly higher hydroxyl group content. With increasing proportions of ferrihydrite in the associations, a corresponding increase in acid consumption was seen, indicating a higher hydroxyl content in ferrihydrite compared with kaolinite within these associations. Further analysis demonstrated that the acid consumption for each association exceeded the value anticipated by the proportional sum of ferrihydrite and kaolinite. Specifically, the acid consumption for the 10% Fhy–Kln, 30% Fhy–Kln, and 50% Fhy–Kln associations was 2.35, 1.74, and 1.32 times greater than the calculated values (see Table S2 in the Supplementary material), respectively. As the proportion of ferrihydrite increased, the acid consumption of the same amount of ferrihydrite in the three associations systems decreased gradually, but it remained greater than that of pure ferrihydrite. These findings indicate that an increase in the proportion of ferrihydrite within the associations leads to a diminished influence of kaolinite on the formation of these associations. The greater presence of kaolinite may enhance the dispersion and reduce the size of ferrihydrite particles during the formation of associations, aligning with the findings from SEM analysis.

FTIR analysis

The interaction between ferrihydrite and kaolinite in the associations was further examined using FTIR. The distributions of characteristic bands of ferrihydrite and kaolinite are shown in Tables S3 and S4 (in the Supplementary material), respectively.

https://doi.org/10.1017/cmn.2024.15 Published online by Cambridge University Press

The FTIR spectra (Fig. 2c) of the minerals revealed that vibration bands (3393 and 3425 cm^{-1}) attributed to the hydroxyl groups of the ferrihydrite structure are evident in the infrared spectra of 30% Fhy–Kln and 50% Fhy–Kln associations. Furthermore, the FTIR spectra observed that the frequencies of the Fhy–Kln associations in the characteristic spectral bands shifted more strongly than those in the spectra of pure ferrihydrite, suggesting the formation of hydrogen bonds between ferrihydrite and kaolinite. The bands at 1114, 1034, 1010, and 755 cm^{-1} correspond to the O-Al-O stretching vibrations, Si-O-Si antisymmetric stretching vibrations, Si-O-Si symmetric stretching vibrations, and Al-O-Si in-plane bending vibrations of kaolinite, respectively. Observations of these bands shifting to lower frequencies in the associations suggest the formation of Al-O-Fe and Si-O-Fe bonds between kaolinite and ferrihydrite (Han et al., 2024; Zeng et al., 2023).

In summary, the presence of kaolinite influenced the properties of ferrihydrite within the associations. Notably, the presence of kaolinite led to a reduction in the aggregation of ferrihydrite, resulting in a more dispersed distribution of ferrihydrite on the surface of kaolinite. Moreover, kaolinite contributed to a decrease in the particle size of ferrihydrite in the associations and an increase in the number of hydroxyl groups on the surface of ferrihydrite. The formation of hydrogen and coordination bonds between kaolinite and ferrihydrite within the associations was also observed. These changes in properties, along with the development of covalent bonds, could consequently have a significant impact on the transformation process of ferrihydrite.

Fe^{2+}-catalyzed transformation of ferrihydrites in associations under various conditions

Reactions of various ferrihydrite–kaolinite associations

The XRD pattern changes over time for Fhy–Kln and Fhy systems under controlled conditions of 0.5 mM Fe^{2+} and pH 7 (Fig. 3) showed that ferrihydrite was transformed into goethite and lepidocrocite. In the Fhy system (Fig. 3a), lepidocrocite alone formed after 4 h of reaction, with its diffraction peak increasing progressively over reaction time. In the 10% Fhy–Kln system (Fig. 3b), the formation of goethite was observed at 24 h, and its diffraction peak intensified after 96 h. In the 30% Fhy–Kln and 50% Fhy–Kln (Fig. 3c,d), the transformation of ferrihydrite to goethite occurred at 4 h, lepidocrocite formed after 24 h, and the diffraction peaks of both goethite and lepidocrocite were further enhanced by 96 h. The results indicate that the presence of kaolinite in the associations promotes the transformation of ferrihydrite into goethite, an effect that becomes more pronounced as the amount of kaolinite in the associations increases. The TEM images after 96 h of reaction in the four systems (Fig. 4) showed the morphologies of the transformed products. The primary transformation products in the Fhy system are predominantly large and massive lepidocrocite (Fig. 4a).

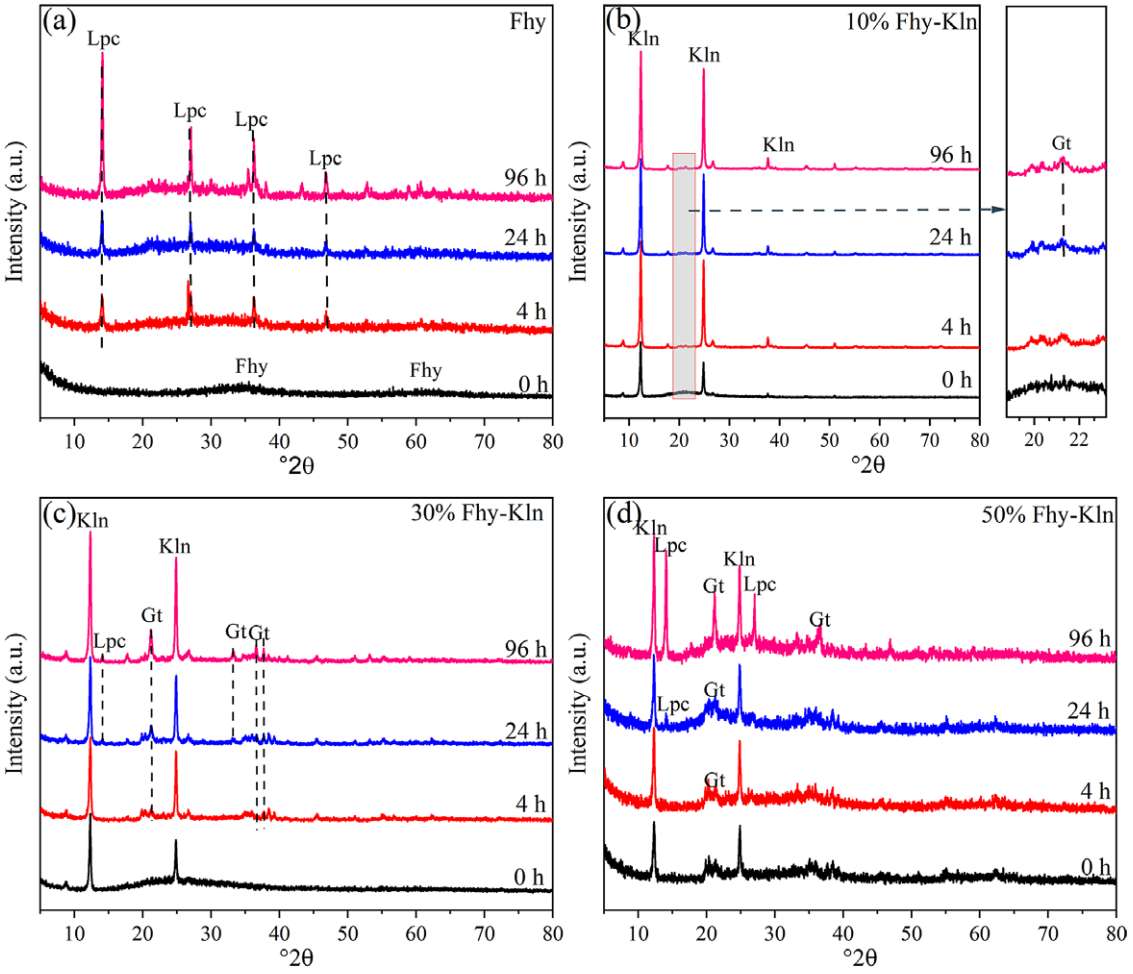

Figure 3. XRD patterns of Fhy and Fhy–Kln associations at pH 7.5 with 0.5 mM Fe^{2+}. (a) Fhy; (b) 10% Fhy–Kln; (c) 30% Fhy–Kln; (d) 50% Fhy-Kln (Fhy, Lpc, Gt, and Kln in XRD patterns were ferrihydrite, lepidocrocite, goethite, and kaolinite, respectively).

https://doi.org/10.1017/cmn.2024.15 Published online by Cambridge University Press

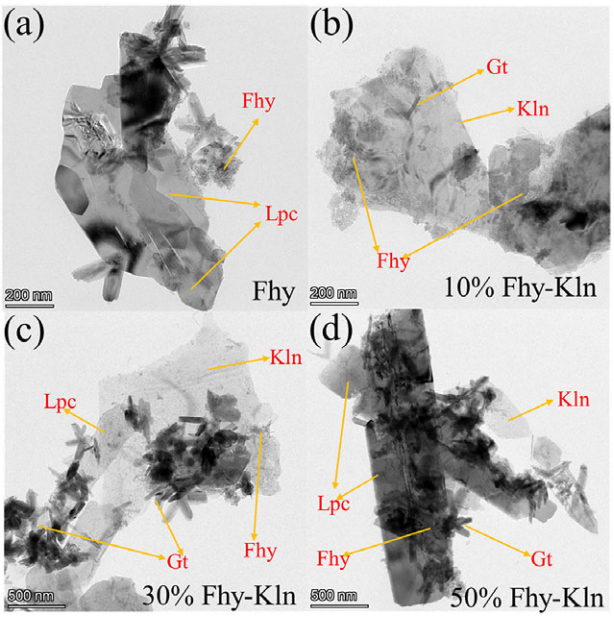

Figure 4. TEM images after a 96 h transformation of (a) Fhy, (b) 10% Fhy–Kln, (c) 30% Fhy–Kln, and (d) 50% Fhy–Kln with 0.5 mM Fe^{2+} at pH 7.5 (Fhy, Lpc, Gt, and Kln in the TEM images represent ferrihydrite, lepidocrocite, goethite, and kaolinite, respectively).

Conversely, in the 10% Fhy–Kln system, granular ferrihydrite is observed, with a minor presence of needle-shaped goethite (Fig. 4b). This observation suggests that the transformation process for ferrihydrite is slow, aligning with the results of the chemical analysis. In the 30% Fhy–Kln and 50% Fhy–Kln systems, large massive lepidocrocite and concurrently formed lath-shaped goethite were observed (Fig. 4c and Fig. 4d), demonstrating morphological variations in the transformation products of ferrihydrite within these associations. The results observed in TEM are consistent with the results obtained from XRD testing. These morphological differences could influence their adsorption capacities, aggregation behavior, and other characteristics, thereby playing distinct roles in modulating the cycling of soil nutrients and pollutants. The rate of ferrihydrite transformation in each system (Fig. S4a) indicates that the process in the Fhy system is quicker than in the association systems. With a greater proportion of kaolinite in the associations, a reduction in transformation of ferrihydrite is observed, particularly evident in the 10% Fhy–Kln system. After 96 h, the transformation percentages for the Fhy, 10% Fhy–Kln, 30% Fhy–Kln, and 50% Fhy–Kln systems are 89.2%, 82.3%, 78.8%, and 25.2% respectively, showing that increasing kaolinite quantity in the system hinders transformation of ferrihydrite. Fe^{2+} dynamics in the solution for each system (Fig. S4b) indicate rapid Fe^{2+} adsorption by the minerals within the first 4 h. As the reaction continues, Fe^{2+} is released back into the solution in the Fhy, 30% Fhy–Kln, and 50% Fhy–Kln systems. Initially, Fe^{2+} is absorbed by either ferrihydrite or kaolinite, but as ferrihydrite transforms into lepidocrocite or goethite, the minerals exhibit a weaker adsorption capacity, resulting in the re-release of Fe^{2+}. The presence of kaolinite in 30% Fhy–Kln and 50% Fhy–Kln systems results in a smaller Fe^{2+} release compared to the Fhy systems. The 10% Fhy–Kln system showed no Fe^{2+} release due to a transformation rate of ferrihydrite and the significant presence of kaolinite, which secures Fe^{2+}. These results indicate that the presence of kaolinite delays the transformation of ferrihydrite, with the inhibitory effect more pronounced at higher kaolinite concentrations. Kaolinite facilitates the transformation of ferrihydrite to goethite, and when the kaolinite content in the associations reaches 90%, only goethite is formed in the system.

Effects of pH

The XRD patterns of the 50% Fhy–Kln and Fhy systems at pH 5.5 after 96 h (see Fig. S5a,c in the Supplementary material) showed that no new iron oxide diffraction peaks were observed. During this period, the transformation rate of ferrihydrite is < 10% (Fig. S6b in the Supplementary material), and the absence of new diffraction peaks in the XRD results suggests the transformation might have been below the detection threshold. The slow transformation rate of ferrihydrite at pH 5.5 is probably due to the low adsorption capacity of the mineral for Fe^{2+} (Fig. S6a in the Supplementary material), resulting in Fe^{2+} predominantly remaining in solution with minimal catalytic efficiency. At pH 6.5, both the 50% Fhy–Kln and Fhy systems produced the same type of transformation products, with the formation of lepidocrocite and goethite starting at 24 h and an increase in their diffraction peaks by 96 h (Fig. S5b,d in the Supplementary material). The 50% Fhy–Kln system revealed a faster transformation rate than the Fhy system at pH 6.5 (Fig. S6c in the Supplementary material), attributed to the greater adsorption of Fe^{2+} in the 50% Fhy–Kln system (Fig. S6a in the Supplementary material). The presence of smaller particles and an increased number of hydroxyl groups on the surface of ferrihydrite in the 50% Fhy–Kln system enhances its adsorption capacity compared with pure ferrihydrite. The results and discussion of the Fhy and 50% Fhy–Kln systems under pH 7.5 reaction conditions are as shown in Fig. 3c, and Fig. S6d in the Supplementary material. The findings demonstrate that change in the properties of ferrihydrite significantly influence its Fe^{2+}-catalyzed transformation of ferrihydrite. With a minimal adsorption of Fe^{2+} (~0.2 mM), the 50% Fhy–Kln system exhibits a faster transformation of ferrihydrite due to its greater adsorption capacity, overcoming the inhibitory effect of kaolinite. However, when the adsorption of Fe^{2+} is equivalent, kaolinite in the 50% Fhy–Kln system also inhibits the transformation of ferrihydrite, resulting in a slower transformation rate compared with the Fhy system.

Effects of initial Fe^{2+} concentration

The changes in the XRD patterns of the Fhy and 50% Fhy–Kln systems with time under reaction conditions of various Fe^{2+} concentrations and pH 7.5 (Fig. S7 in the Supplementary material) revealed that the transformation of ferrihydrite differed. When the concentration of Fe^{2+} was 0.5 mM, both lepidocrocite and goethite were formed in the 50% Fhy–Kln system (Fig. 3c), while only lepidocrocite was formed in the Fhy system (Fig. 3d). At a concentration of 1 mM Fe^{2+} (Fig. S7a,c in the Supplementary material), lepidocrocite was produced exclusively in the Fhy system after 24 h, whereas only goethite was produced in the 50% Fhy–Kln system. By 96 h, the Fhy system showed an increased diffraction peak of lepidocrocite, while in the 50% Fhy–Kln system, the goethite diffraction peak was enhanced, and both lepidocrocite and magnetite were observed. Increasing the Fe^{2+} concentration to 2 mM (Fig. S7b,d in the Supplementary material) led to the production of lepidocrocite in the Fhy system and goethite in the 50% Fhy–Kln system at 4 h. By 96 h, the diffraction peak of lepidocrocite in the Fhy system decreased, and a diffraction peak for magnetite emerged. Conversely, in the 50% Fhy–Kln system, the diffraction peak for goethite intensified, and the diffraction peak for magnetite appeared simultaneously. These results indicate a differential formation process for magnetite in between the Fhy

https://doi.org/10.1017/cmn.2024.15 Published online by Cambridge University Press

and 50% Fhy–Kln systems. In the Fhy system, ferrihydrite first transformed into lepidocrocite, which then transformed into magnetite. In contrast, in the 50% Fhy–Kln system, magnetite formation occurred directly through the dissolution and precipitation of ferrihydrite. The transformation rates of ferrihydrite varied with different concentrations of Fe^{2+}. Specifically, at 0.5 mM Fe^{2+} (Fig. S8b in the Supplementary material), the transformation rate was faster in the Fhy system compared with the 50% Fhy–Kln system. However, when the concentration of Fe^{2+} increases to 1 and 2 mM (Fig. S8c,d in the Supplementary material), the transformation rate of the Fhy system becomes slower than that of the 50% Fhy–Kln system. This may be attributed to the various transformation pathways of ferrihydrite in the system. When magnetite was produced directly from ferrihydrite, the transformation rate of ferrihydrite increased. As the initial Fe^{2+} concentration of the reaction increased, the amount of Fe^{2+} adsorbed in each system also increased (Fig. S8a in the Supplementary material). However, the difference in the transformation rate of ferrihydrite was not significant, indicating that once the surface Fe(II) concentration of ferrihydrite reached a certain level, the transformation rate of ferrihydrite did not increase with increasing surface Fe(II) quantity. Additionally, the reaction of 1 and 2 mM Fe^{2+} did not result in the re-release of Fe^{2+} because a portion of the Fe(II) was incorporated into the structure of magnetite. These results demonstrate that the presence of kaolinite alters the transformation pathway of ferrihydrite to magnetite in the associations system and results in a faster transformation rate than in the Fhy system.

Transformation of ferrihydrite in the mixed system

In an investigation to assess the effect of kaolinite on the transformation pathway of ferrihydrite within the associated system, a series of Fe^{2+} catalytic experiments of the mixed system were performed. The mixed system consisted of 0.5 g L^{-1} ferrihydrite and 0.5 g L^{-1} kaolinite, each added separately (Fig. 5). At pH 7.5, with 0.5 mM Fe^{2+} or 1 mM Fe^{2+}, ferrihydrite in the mixed system only transformed into lepidocrocite. At the same pH, but with 2 mM Fe^{2+}, ferrihydrite in the mixed system underwent transformation into both lepidocrocite and magnetite. At pH 6.5, with 0.5 mM Fe^{2+}, the transformation resulted in the formation of lepidocrocite and goethite. Comparison of XRD patterns between the associated system and the Fhy system revealed that the transformation pathway of ferrihydrite in the mixed system paralleled that of the Fhy system. This indicates that the variation in the transformation of ferrihydrite in the associated and the mixed system is not influenced by kaolinite but is determined by the intrinsic properties of ferrihydrite. Additionally, the transformation rate of ferrihydrite in each mixed system was lower compared with both the associated and the Fhy system (Fig. S9 in the Supplementary material), indicating that the presence of kaolinite in the mixed system inhibits the transformation of ferrihydrite. The accelerated transformation of ferrihydrite in the co-existing system is ascribed to changes in the properties of ferrihydrite, which counteract the inhibitory effect of kaolinite, leading to a faster transformation process compared with the Fhy system. The increased transformation rate of ferrihydrite in the associated system relative to the mixed system could be attributed to differences in Fe^{2+} adsorption efficiency. Ferrihydrite in the mixed system exhibits a lower Fe^{2+} compared with the associated system (Fig. S10 in the Supplementary material), due to the greater presence of hydroxyl groups on the surface of ferrihydrite in the associated system (Fig. S11 in the Supplementary material), facilitating greater Fe^{2+} adsorption. This increased surface-adsorbed Fe^{2+} and the interfacial electron transfer between ferrihydrite–Fe(III) promote the more rapid transformation of ferrihydrite.

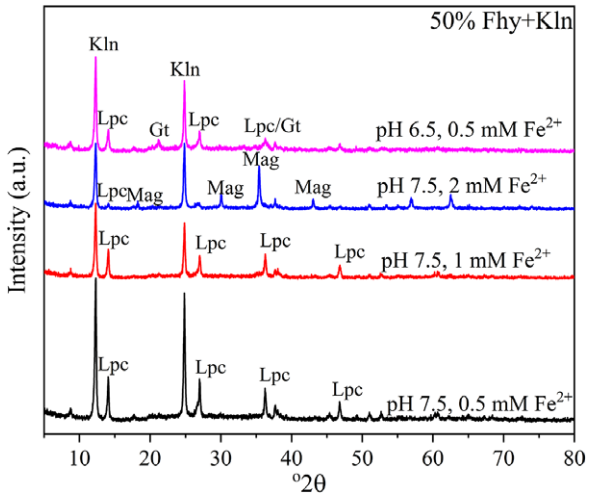

Figure 5. XRD patterns of a 50% Fhy–Kln system at various reaction conditions (Lpc, Gt, Mag, and Kln in XRD patterns represent lepidocrocite, goethite, magnetite, and kaolinite, respectively).

Conclusions

The research results confirm the hypothesis that the relative proportions of kaolinite, concentration of Fe^{2+}, and pH are pivotal in determining the formation of specific Fe-(oxyhydr) oxides. Variations in Fe^{2+} concentration and pH markedly influence both the transformation pathways and the rate of ferrihydrite's transformation. Furthermore, an increase in kaolinite content correlates with a greater specific surface area of the associations, resulting in a greater number of hydroxyl groups on the surface. This enhanced transformation rate in the associations is attributed to the smaller size of ferrihydrite particles and the increased presence of hydroxyl groups on the surface of ferrihydrite, which promotes more Fe^{2+} adsorption, thereby accelerating the transformation rate of ferrihydrite. Additionally, the presence of kaolinite promotes the formation of goethite. During the formation of goethite, heavy-metal pollutants are incorporated into the crystal lattice and immobilized, and this process can markedly reduce the effectiveness of heavy-metal elements. These observations lay a theoretical groundwork for further studies on the transformation of ferrihydrite in mineral environments within anoxic conditions, such as paddy fields and wetlands, facilitating a deeper understanding of their roles and impacts in such ecosystems.

Supplementary material. The supplementary material for this article can be found at http://doi.org/10.1017/cmn.2024.15.

Author contribution. Cong Wu: Writing-original draft, Methodology, Investigation. Shuai Wang: Methodology, Investigation. Wenjuan Liao: Methodology, Formal analysis. Hao-Jie Cui: Writing-review & editing, Funding acquistion, Conceptualization.

Acknowledgements. None.

Data availability statement. Data will be made available on request.

Financial support. This work was supported by the Natural Science Foundation of China (grant nos. 42277291 and 41771272), and the Opening Fund of the State Key Laboratory of Environmental Geochemistry (SKLEG2023202).

Competing interests. On behalf of all authors, the corresponding author states that there are no competing interests.

References

Aeppli, M., Kaegi, R., Kretzschmar, R., Voegelin, A., Hofstetter, T.B., & Sander, M. (2019). Electrochemical analysis of changes in iron oxide reducibility during abiotic ferrihydrite transformation into goethite and magnetite. *Environmental Science & Technology*, *53*, 3568–3578. https://doi.org/10.1021/acs.est.8b07190

Bhattacharyya, K.G., & Gupta, S.S. (2009). Calcined tetrabutylammonium kaolinite and montmorillonite and adsorption of Fe(II), Co(II) and Ni(II) from solution. *Applied Clay Science*, *46*, 216–221. https://doi.org/10.1016/j.clay.2009.08.006

Cai, X., ThomasArrigo, L.K., Fang, X., Bouchet, S., Cui, Y., & Kretzschmar, R. (2020). Impact of organic matter on microbially-mediated reduction and mobilization of arsenic and iron in arsenic(V)-bearing ferrihydrite. *Environmental Science & Technology*, *55*, 1319–1328. https://doi.org/10.1021/acs.est.0c05329

Day, P.R. (1965). Particle fractionation and particle-size analysis. *Methods of Soil Analysis*, *9*, 545–567. https://doi.org/10.2134/agronmonogr9.1.c43

Eren, E., & Afsin, B. (2008). An investigation of Cu(II) adsorption by raw and acid-activated bentonite: a combined potentiometric, thermodynamic, XRD, IR, DTA study. *Journal of Hazardous Materials*, *151*, 682–691. https://doi.org/10.1016/j.jhazmat.2007.06.040

Fan, Q., Wang, L., Fu, Y., & Wang, Z. (2023). Impacts of coexisting mineral on crystallinity and stability of Fe(II) oxidation products: implications for neutralization treatment of acid mine drainage. *Journal of Hazardous Materials*, *442*, 130060. https://doi.org/10.1016/j.jhazmat.2022.130060

Gilkes, R.J., & Nattaporn P. (2016). How the unique properties of soil kaolin affect the fertility of tropical soils. *Applied Clay Science*, *131*, 100–106. https://doi.org/10.1016/j.clay.2016.01.007

Gu, Q., Liu, J., Yang, Y., Zhu, R., Ma, L., Liang, X., Long, S., Zhu, J., & He, H. (2022). The different effects of sulfate on the adsorption of REEs on kaolinite and ferrihydrite. *Applied Clay Science*, *221*, 106468. https://doi.org/10.1016/j.clay.2022.106468

Gu, X., & Evans, L.J. (2008). Surface complexation modelling of Cd(II), Cu(II), Ni(II), Pb(II) and Zn(II) adsorption onto kaolinite. *Geochimica et Cosmochimica Acta*, *72*, 267–276. https://doi.org/10.1016/j.gca.2007.09.032

Han, B., Liu, J., Zhu, R., & Chen, Q. (2024). Clay minerals inhibit the release of Cd(II) during the phase transformation of Cd(II)-ferrihydrite coprecipitates. *Journal of Hazardous Materials*, *462*, 132723. https://doi.org/10.1016/j.jhazmat.2023.132723

Hansel, C.M., Benner, S.G., & Fendorf, S. (2005). Competing Fe(II)-induced mineralization pathways of ferrihydrite, *Environmental Science & Technology*, *39*, 7147–7153. https://doi.org/10.1021/es050666z

Hu, Y., Xue, Q., Tang, J., Fan, X., & Chen, H. (2019). New insights on Cr(VI) retention by ferrihydrite in the presence of Fe(II). *Chemosphere*, *222*, 511–519. https://doi.org/10.1016/j.chemosphere.2019.01.160

Huang, B., Yuan, Z., Li, D., Zheng, M., Nie, X., & Liao, Y. 2020. Effects of soil particle size on the adsorption, distribution, and migration behaviors of heavy metal(loid)s in soil: a review. *Environmental Science: Processes & Impacts*, *22*, 1596–1615. https://doi.org/10.1039/D0EM00189A

Iorio, E.D., Circelli, L., Angelico, R., Torrent, J., Tan, W., & Colombo, C. (2022). Environmental implications of interaction between humic substances and iron oxide nanoparticles: a review. *Chemosphere*, *303*, 135172. https://doi.org/10.1016/j.chemosphere.2022.135172

Kuila, U., & Prasad, M. (2013). Specific surface area and pore-size distribution in clays and shales. *Geophysical Prospecting*, *61*, 341–362. https://doi.org/10.1111/1365-2478.12028

Laurel, K.T., Ralf, K., & Ruben, K. (2019). Ferrihydrite growth and transformation in the presence of ferrous iron and model organic ligands. *Environmental Science & Technology*, *53*, 13636–13647. https://doi.org/10.1021/acs.est.9b03952

Liu, Y., Ding, Y., Sheng, A., Li, X., Chen, J., Arai, Y., & Liu, J. (2023). Fe(II)-catalyzed transformation of ferrihydrite with different degrees of crystallinity. *Environmental Science & Technology*, *57*, 6934–6943. https://doi.org/10.1021/acs.est.3c00555

Mendez, J.C., Tjisse, H., & Gerwin, F.K. (2020). Assessing the reactive surface area of soils and the association of soil organic carbon with natural oxide nanoparticles using ferrihydrite as proxy. *Environmental Science & Technology*, *54*, 11990–2000. https://doi.org/10.1021/acs.est.0c02163

Meng, F., Bu, H., Fei, Y., Chen, M., Lei, Q., Liu, D., Hua, J., Wu, F., & Liu, C. (2022). Effects of clay minerals on Fe^{2+}-induced phase transformation of ferrihydrite. *Applied Geochemistry*, *144*, 105401. https://doi.org/10.1016/j.apgeochem.2022.105401

Ryan, P.C., & Javier, H.F. (2013). Reaction pathways of clay minerals in tropical soils: insights from kaolinite-smectite synthesis experiments. *Clays and Clay Minerals*, *61*, 303–318. https://doi.org/10.1346/CCMN.2013.0610410

Schwertmann, U., & Cornell, R.M. (2008). *Iron Oxides in the Laboratory: Preparation and Characterization*. John Wiley & Sons.

Sheng, A., Liu, J., Li, X., Qafoku, O., Collins, R.N., Jones, A.M., Pearce, C.I., Wang, C., Ni, J., Lu, A., & Rosso, K.M. (2020). Labile Fe(III) from sorbed Fe(II) oxidation is the key intermediate in Fe(II)-catalyzed ferrihydrite transformation. *Geochimica et Cosmochimica Acta*, *272*, 105–120. https://doi.org/10.1016/j.gca.2019.12.028

Shi, M., Min, X., Ke, Y., Lin, Z., Yang, Z., Wang, S., Peng, N., Yan, X., Luo, S., Wu, J., & Wei, Y. (2021). Recent progress in understanding the mechanism of heavy metals retention by iron (oxyhydr)oxides. *Science of the Total Environment*, *752*, 141930. https://doi.org/10.1016/j.scitotenv.2020.141930

Stookey, L.L. (1970). Ferrozine – a new spectrophotometric reagent for iron. *Analytical Chemistry*, *42*, 779–781. https://doi.org/10.1021/ac60289a016

Sun, Z., Zhu, R., Ding, T., Zhang, X., & Li, C. (2022). Induced morphology orientation of alpha-FeOOH by kaolinite for enhancing peroxymonosulfate activation. *Journal of Colloid and Interface Science*, *626*, 494–505. https://doi.org/10.1016/j.jcis.2022.06.151

Thommes, M., Kaneko, K., Neimark, A.V., Olivier, J.P., Rodriguez-Reinoso, F., Rouquerol, J., & Sing, K.S.W. (2015). Physisorption of gases, with special reference to the evaluation of surface area and pore size distribution (IUPAC Technical Report). *Pure and Applied Chemistry*, *87*, 1051–1069. https://doi.org/10.1515/pac-2014-1117

Van, G.N., ThomasArrigo, L.K., Byrne, J.M., Kappler, A., Christl, I., & Kretzschmar, R. (2020). Interactions of ferrous iron with clay mineral surfaces during sorption and subsequent oxidation. *Environmental Science: Processes & Impacts*, *22*, 1355–1367. https://doi.org/10.1039/d0em00063a

Wang, X., Zhu, M., Luuk, K.K., Li, W., Xu, W., Liu, F., Zhang, J., Liu, Q., Feng, X., & Sparks, D.L. (2016). Effects of crystallite size on the structure and magnetism of ferrihydrite. *Environmental Science: Nano*, *3*, 190–202. https://doi.org/10.1039/C5EN00191A

Wei, S., Liu, F., Feng, X., Tan, W., & Koopal, L.K. (2011). Formation and transformation of iron oxide-kaolinite associations in the presence of iron(II). *Soil Science Society of America Journal*, *75*, 45–55. https://doi.org/10.2136/sssaj2010.0175

Wei, S., & Yang, X. (2010). Surface properties and adsorption characteristics for fluoride of goethite, kaolinite and their association. *Environmental Science*, *31*, 2134–2142. https://doi.org/10.13227/j.hjkx.2010.09.025

Yan, L., Chen, Q., Yang, Y., & Zhu, R. (2021). The significant role of montmorillonite on the formation of hematite nanoparticles from ferrihydrite under heat treatment. *Applied Clay Science*, *202*, 10562. https://doi.org/10.1016/j.clay.2020.105962

Zeng, L., Li, X., Jiang, F., Yin, M., Dang, Z., Zhang, L., Huang, W., & Yi, X. (2023). The effect of kaolinite on ferrihydrite colloid migration in soil: molecular-scale mechanism study. *Environmental Science: Nano*, *10*, 2754–2766. https://doi.org/10.1039/d3en00333g

Zhang, L., Fu, F., Peng, J., & Tang, B. (2023a). The mobility of Cr(VI) on the ferrihydrite-Cr(VI) co-precipitates: the effect of co-existing tartaric acid and Cu(II). *Applied Geochemistry*, *152*, 105646. https://doi.org/10.1016/j.apgeochem.2023.105646

Zhang, T., Tang, B., & Fu, F. (2023b). Influence of montmorillonite incorporation on ferrihydrite transformation and Cr(VI) behaviors during ferrihydrite-Cr(VI) coprecipitates aging. *Science of the Total Environment*, *873*, 162257. https://doi.org/10.1016/j.scitotenv.2023.162257

Zhao, X., Yuan, Z., Wang, S., Zhang, G., Qu, S., Wang, Y., Liu, S., Pan, Y., Lin, J., & Jia, Y. (2022a). The fate of co-existent cadmium and arsenic during Fe(II)-induced transformation of As(V)/Cd(II)-bearing ferrihydrite. *Chemosphere*, *301*, 134665. https://doi.org/10.1016/j.chemosphere.2022.134665

Zhao, X., Yuan, Z., Wang, S., Pan, Y., Chen, N., Tunc, A., Cheung, K., Alparov, A., Chen, W., Deevsalar, R., Lin, J., & Jia, Y. (2022b). Iron(II)-activated phase transformation of Cd-bearing ferrihydrite: implications for cadmium mobility and fate under anaerobic conditions. *Science of the Total Environment*, *848*, 157719. https://doi.org/10.1016/j.scitotenv.2022.157719

Zhou, Z., Latta, D.E., & Scherer, M.M. (2021). Natural organic matter inhibits Ni stabilization during Fe(II)-catalyzed ferrihydrite transformation. *Science of the Total Environment*, *755*, 142612. https://doi.org/10.1016/j.scitotenv.2020.142612

https://doi.org/10.1017/cmn.2024.15 Published online by Cambridge University Press